DIFFERENTIAL SEMI-QUANTITATIVE URBAN RISK ASSESSMENT OF STORM SURGE INUNDATION

Yuewei Wang[1], Xiaodao Chen[1], Lizhe Wang[1] *

[1] School of Computer Science, China University of Geosciences, Wuhan, Hubei, 430078, P.R.China.
yuewei.w@cug.edu.cn, , xiaodao_chen@foxmail.com, lizhe.wang@gmail.com

KEY WORDS: Storm Surge Inundation, Risk Assessment, Digital Twin, Semi-Quantitative Risk Assessment

ABSTRACT:

Storm surge inundation hazards annually cause billions in economic losses globally, and millions of coastal residents live in danger. Properly understanding and assessing storm surge inundation are essential measures to guarantee the sustainable construction of coastal cities. In this paper, a differentiated urban risk semi-quantitative assessment method for storm surge inundation is proposed to evaluate the risk of storm surge hazard causing inundation to the coastal city. The Finite Volume Community Ocean Model (FVCOM) and the Jelesnianski model restore the historical storm surge cases to reveal hazards. The point of interest data and the urban land use and land cover data are utilized to assess the vulnerability of the coastal city, and a differentiated risk assessment method is proposed to evaluate the risks for urban facilities in the hazard. As an illustration, the method is utilized to assess storm surge Mangkhut in 2018 in Shenzhen, Guangdong Province, China. The vulnerability of the Shenzhen downtown area is assessed and designed as a map to visualize the strategic area. According to numerical simulation and inundation region mapping, the danger and the risk assessment map are made to intuitively present the distribution of the hazard-affected region.

1. INTRODUCTION

Storm surge, which is caused by violent atmospheric disturbances, constantly threatens coastal cities. Affected by wind moving cyclonically around a storm, the hazard breaks coastal barriers and pushes water into the shoreside, causing severe urban inundation (Dube et al., 2004). From 1880 to 2015, more than 700 storm surge hazards were recorded, and the hazard inundation annually caused billions of dollars in losses and severe personal casualty losses worldwide. Over 600 million people are exposed to storm surge hazards because they live in low-lying coastal areas, and on average 0.8 to 1.1 million people are affected by inundation (McGranahan et al., 2007, Hinkel et al., 2014). Powerful hazard cause widespread concerns in the international community. An approach that models the inundation hazard and extracts the inner principle of the evolution process can work auxiliary to support hazard prevention decisions. For frequently aroused hazards, an effective method for understanding storm surge inundation has become a significant issue in the development of coastal cities.

Storm surge inundation, which changes rapidly and has wide effects, is a complex natural phenomenon. One way to understand hazards is to study historical statistics about hazards (Zachry et al., 2015, Ceres et al., 2017). However, due to the limited, partly inaccurate statistics available, research conclusions can be inevitably misled. Certain features of data create obstacles to further investigation of historical storm surge inundation. One issue is low-resolution data. Storm surge hazards with changing rapidly, affecting a wide range of features, make comprehensive monitoring difficult. Water levels cannot be logged in high spatial resolution and temporal resolution (Shen and Chang, 2013). Another issue is unreliable statistical data. Statistical authority is a response to hazard investigations. The human error involved in data collection is unpreventable and unpredictable (Chen and BAI, 2011). By leveraging the Remote Sensing (RS) technique, marine satellites provide more historical data. However, due to the inclement weather conditions, the validity of RS data is hard to guarantee. Therefore, advanced techniques have to be introduced to achieve the risk assessment.

The research on hazard risk assessment is an emerging topic from the twentieth century (Zhang and Chen, 2019). Hazard risk assessment methods can be classified into four different methods: statistics methods, indicator methods, RS and geographic information system methods, and numerical methods. Statistical methods extract patterns based on a large amount of historical data. It can distinctly illustrate a hazard-affected region (Polomčić et al., 2018). The indicator methods evaluate the hazard based on the analysis of the diversity influence factors. A couple of hazard-involved factors is taken into consideration, and the influence weight of each factor is assigned by the correlation analysis method (Liu et al., 2020). These two methods conclude that the analytical results rely on historical data. Imprecise statistics can easily mislead final conclusions. RS and geographic information system techniques take advantage of graphic information systems to process RS data to map the distribution of the inundation situation in a city (Zheng et al., 2010). Storm surge hazards are mostly accompanied by heavy rainfall, and weather conditions can severely influence RS data quality. RS satellites have their corresponding revisit period, so they cannot continually monitor a hazard region. The numerical simulation methods reproduce hazards based on marine environmental data according to a series of dynamic equations (Xianwu et al., 2020). Based on the RS data, the researches on numerical simulation dedicate to understand the mechanism of storm surge hazard, and offer a prospect for the precise risk assessment in a challenging urban environment.

A Differentiated Semi-quantitative Urban Risk Assessment Method (DSURAM) of storm surge inundation is proposed in this paper under the digital twin framework. The methodology researches the entire workflow to digitalize storm surge hazards in two steps, simulation and assessment. The unstructured-grid-

* Corresponding author

This contribution has been peer-reviewed. The double-blind peer-review was conducted on the basis of the full paper.
https://doi.org/10.5194/isprs-annals-X-3-W1-2022-177-2022 | © Author(s) 2022. CC BY 4.0 License.

based marine numerical simulation model, the FVCOM and the cyclone wind model, the Jelesnianski model, are coupled for a storm-surge-hazard-caused inundation simulation. A differentiated risk semi-quantitative assessment method is proposed to determine the vulnerability of each urban Land Use and Land Cover (LULC) based on the official standard and multi-source urban data. Then, the disaster intensity and corresponding risk assessment can be evaluated by the proposed method to support hazard prevention decisions. The contributions of this paper are summarized as follows.

- A digital twin of storm surge inundation in the coastal city is proposed to integrate the disaster simulation, urban vulnerability, disaster risk assessment into a whole.
- A differentiated risk assessment method is designed to assess each LULC area's vulnerability, danger, and risk in a storm surge hazard by blending the official principle and multiple urban data.
- Targeting to the storm surge Mangkhut in September 2018, a case study is conducted to reproduce the hazard evolution and hazardous situation in Shenzhen, China.

The rest of the paper is organized as follows. Section 2 defines the targeting assessment problem of the storm surge inundation in detail. Section 3 introduces the study area and the corresponding dataset utilized in this work. Section 4 presents the DSURAM in details. Section 5 presents a case study in Shenzhen, Guangdong Province, China, for the storm surge Mangkhut in 2018 with analysis. A summary of the work is given in Section 6.

2. PROBLEM DEFINITION

Storm surge inundation is a natural disaster with a wide range, multiple processes, and complex mechanisms. Abstracting the disaster-causing process and defining the boundaries of the assessment problem is vital for hazard analysis. Storm surge disaster risk assessment is generally divided into two modules, simulation and assessment. These two modules are in a sequential relationship. The simulation module reproduces the evolution of the disaster. Based on the inundation status, an assessment principle is designed and constructed to perform precise risk assessment on urban features.

The data required in the simulation module can be classified as the historical marine environmental data and meteorological data. The marine environmental data include the coastline, topography, tidal information, temperature, and salinity. The meteorological data include the trajectory, moving speed, center pressure, and maximum wind speed of the storm surge hazard. These data can present the storm surge evolution in different aspects. We would like to reproduce every evolution detail in the hazard and obtain the inundation depth over the whole research region. The method that can precisely simulate the storm surge evolution is the primary issue in this module.

To assess storm surge inundation status, urban data are necessary for the risk assessment target. The urban data include the LULC data and the Point of Interest (POI) data. The LULC data present the usage situation for different regions. The POI data present a diversity of landmark locations. The basic information, from the convenience stores to the mall, from the neighborhood committee to the government building, is gathered in the POI data. In addition, the storm surge inundation assessment has an official standard. The official standard stipulates the risk assessment of different land usages. The target is to assess the risks for every LULC in the research region. Therefore, extending the official standard to specified assess each LULC in the research region is vital for a refined risk assessment.

3. STUDY AREA AND DATASET

The proposed method is targeted to digitalize the marine hazard in the specified coastal region. The basic information of research region, Shenzhen, China, is introduced in Section 3.1. The data utilized in this paper are introduced in Section 3.2.

3.1 Study area

Shenzhen is located in the south of China in Guangdong Province. Spanning between 113.43° and 114.38° east longitude and 22.24° and 22.52° north latitude, Shenzhen borders the South China Sea. As shown in Figure 1, the area of Shenzhen is $1,997.47$ km^2 and, for administrative division, Shenzhen can be composed of 10 districts. Half of these include the coastal area, which are the Bo'an district, the Nanshan district, the Futian district, the Yantian district, and the Dapeng new district. The total length of the coastline in Shenzhen is about 230 km.

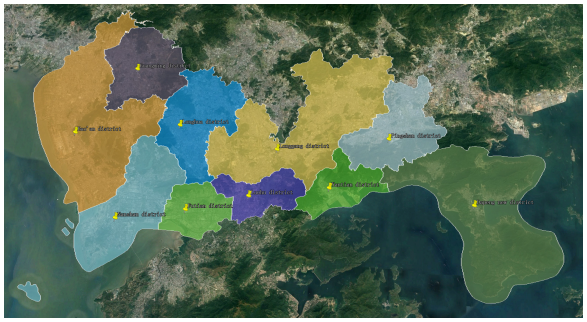

Figure 1. The districts distribution map in the Shenzhen area.

China is at the northwest of the Pacific Ocean for its geographical position. The storm surge hazards generate around the east of the Phillips, the middle of the South Sea, or the west of Japan can potentially to move toward China. From 1949 to 2006, over 500 storm surge hazards landed in China, and over 160 hazards landed in Guangdong Province. As the center of this province's population and economy, Shenzhen is a vulnerable city to disasters and could suffer heavy losses. This paper selected the storm surge Mangkhut in 2018, which severely influenced Shenzhen, for a case study.

3.2 Dataset

Hazard-related data have characteristics of multi-source and heterogeneous. The dataset has to be carded throughout to support the establishment of storm surge inundation assessment. The data utilized for hazard modeling and analysis can be classified as marine, hazard, and urban data. The marine data contains basic marine and geographic information. The storm surge data contains the time series climate information derived from continually monitoring the evolution of the hazard. The urban data include the morphology, LULC, and POI information in the urban area. The details are introduced as follows.

- Marine data: The bathymetric, coastline, and tide information were collected to describe the marine information

in storm surge hazard. The Global Self-consistent, Hierarchical, High-resolution Geography Database (GSHHG) provided global coastline and the political border information. It benefits this work by designing the grid for numerical simulation (Wessel and Smith, 1996). The General Bathymetric Chart of the Oceans (GEBCO), which is gridded bathymetric data with a $15''$ grid of spatial resolution, was utilized for both the marine bathymetric and urban topography data (Kapoor, 1981). The TOPEX/POSEIDON global tidal model v9 atlas (TPXO9-atlas) provided by Oregon State University (OSU) was utilized (Egbert and Erofeeva, 2002). The spatial resolution is $1/30$ degree. Temperature and salinity were customized as default values of $20°$C and 35 Practical Salinity Units (PSU), respectively.

- Storm surge data: The storm surge data represent information about the marine climate. The center of a storm surge can be extremely intense when it arises. In order to reproduce the hazard, the storm surge trajectory, moving direction, moving speed, maximum wind force, and central pressure were obtained from the Central Meteorological Station for hazard simulation. A background wind field dataset, the Cross-Calibrated Multi-Platform (CCMP), was utilized for data fusion requirements. The dataset was collected by the wind satellite supported by the National Aeronautics and Space Administration (NASA). The spatial resolution of the CCMP data is 0.25 degree, and the temporal resolution is six hourly.

- Urban data: Multi-source urban data require to be collected to assess the diversity perspective of the urban area in the storm surge inundation. LULC and POI are the primary issues required to be taken into consideration. The LULC data were provided by the Gong et al. (Gong et al., 2020). The data classify the land cover of all of China, including $440,798$ parcels, into 12 classes. The POI data and the administrative border data were collected from Baidu Map. In addition, to improve the credibility of the assessment result, "Guideline for Risk Assessment and Zoning of Storm Surge Disaster," which was established and published by the State Oceanic Administration, was utilized as the primary reference in the hazard assessment method.

4. PROPOSED METHOD

The DSURAM is presented in detail in this section. The workflow of the hazard assessment architecture is introduced from a high level in Section 4.1. Numerical simulation methods are illustrated in Section 4.2. The proposed assessment system and corresponding method are introduced in Section 4.3.

4.1 A DSURAM framework

With the establishment of the digital twin, new study perspectives have been brought into hazard-related research. The digital twin is a technical framework that clones an object in physical space to digital space for analysis and assessment purposes (Fuller et al., 2020). Following the digital twin concept, the procedure of the hazard assessment is to map the natural phenomenon, storm surge, from the physical space to the digital space as shown in Figure 2. The cyclones cause drastic atmospheric and ocean motion. Intense motion causes the massive tidal wave to crash onto land. The monitoring data are continually collected and transferred to digital space. Numerical methods are utilized to model the dynamic principle and the statistic principle of the hazard. Then, combining the expert experience method and urban data, an assessment is conducted to evaluate the risks in a different region of the urban area. The risk assessment map is designed to intuitively present the stricken distribution and supports hazard prevention decision making.

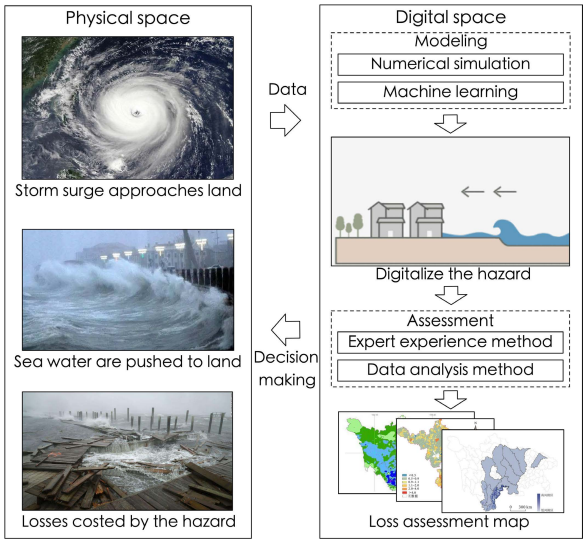

Figure 2. The conceptual framework of the DSURAM.

The technical problem converges on the simulation and assessment methodology in digital space. The proposed technical workflow is shown in Figure 3. The diversity of the data supports the research of the whole workflow. The marine data are fed into the numerical model, the FVCOM, to simulate the tidal evolution during the storm surge hazard. The storm surge data are fed into the wind field model, the Jelesnianski model, to simulate the evolution of the atmosphere during the storm surge hazard. The status of the tide and atmosphere are then coupled together to reproduce the hazard.

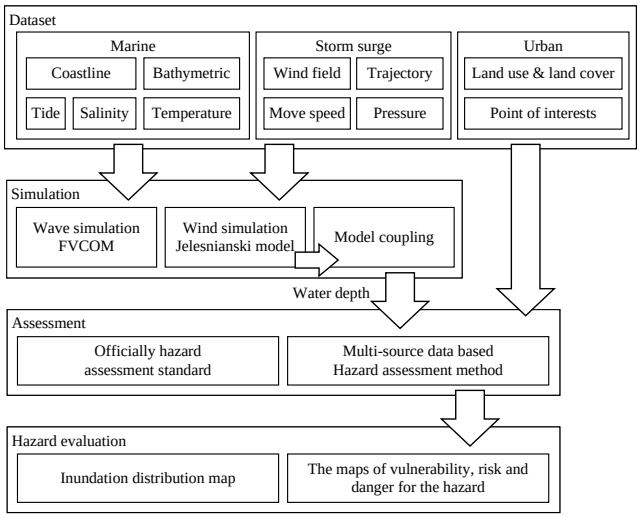

Figure 3. The technical workflow of the DSURAM.

Subsequently, the simulated inundation depth and the urban data are utilized in the risk assessment via multi-scale data fusion. The inundation depth is the common network data form associated with the grid utilized in the simulation. The LULC and POI are correspondingly composed of points and polygons. Under these circumstances, a differential semi-quantitative assessment method is proposed to enhance the official storm surge

hazard assessment standard in precise evaluation. The proposed assessment method, collaborating with POIs, proposes the difference index to elaborately distinguish vulnerability for each LULC. The vulnerability, danger, and risk assessment results are utilized for the assessment map design. The Geographic Information System (GIS) is utilized in graphics.

4.2 Storm surge simulation module

The storm surge hazard is composed of the atmospheric motion and the tidal motion caused by the cyclone. As mentioned in Section 4.1, the tide and wind field are separately utilized by the FVCOM and the Jelesnianski model and coupled together for the simulation requirement.

The Jelesnianski model is utilized to generate the wind field all over the research region at each time. Since the influence of the tropical cyclone is gradually decreased, the background wind field dataset, CCMP, is utilized to rectify the wind field to approach the practical situation. The CCMP data can guarantee the accuracy of normal meteorological conditions, but CCMP data cannot handle extreme cases. The data assimilation of the simulation model and the CCMP data can effectively tackle this issue.

The Jelesnianski model is an empirical model proposed by Jelesnianski, et al., in 1973 to simulate the tropical cyclone in the research region. Compared to other classic synthetic wind field techniques, for instance, Holland, Fujita-Takahashi, the Jelesnianski model is more accurate while simulating cyclones that occur in South Sea (Shi et al., 2018). The Jelesnianski model is composed of the circling wind velocity and the migrating velocity speed, which are formulated as follows.

$$\vec{S_m} = \begin{cases} \frac{D}{D+R}(\vec{V}\cdot\vec{U}) & 0 < D \le R \\ \frac{R}{D+R}(\vec{V}\cdot\vec{U}) & R < D \end{cases} \tag{1}$$

$$\vec{S_c} = \begin{cases} W\left(\frac{D}{R}\right)^{\frac{3}{2}}\vec{V}\frac{\vec{A}\cdot\vec{U}}{D} & 0 < D \le R \\ W\left(\frac{R}{D}\right)^{\frac{1}{2}}\vec{V}\frac{\vec{A}\cdot\vec{U}}{D} & R < D \end{cases} \tag{2}$$

$$P = \begin{cases} P_0 + \frac{1}{4}(P_\infty - P_0)\left(\frac{D}{R}\right)^3 & 0 < D \le R \\ P_\infty - \frac{3}{4}(P_\infty - P_0)\frac{R}{D} & R < D \end{cases} \tag{3}$$

$$\vec{A} = [-D_x \sin\alpha + D_y \cos\alpha, D_x \cos\alpha - D_y \sin\alpha] \\ D_x = x - x_0,\ D_y = y - y_0 \tag{4}$$

where (x, y) and (x_0, y_0) represent the coordinates of the target and cyclone center locations. D represents the Euclidean distance between the cyclone center and target location. α represents the influx angle of surface wind, and in this work, α is customized as $20°$. $\vec{V}$ represents the cyclone moving velocity vector. W represents the current maximum wind speed. P_∞ and P_0 are the pressures of the general atmosphere and the cyclone center. P_∞ is set to be 1013 hPa. R represents the radius of the maximum wind speed. The calculation method for the radius of the maximum wind speed R is proposed by Graham (E and E, 1959).

The data assimilation of the empirical model and the background wind data is calculated as the following equation.

$$r = \left(\frac{D}{10R}\right)^4 \\ \vec{S_t} = \frac{\vec{S_m}+\vec{S_c}}{1+r} + \frac{r\vec{S_g}}{1+r} \tag{5}$$

where $\vec{S_t}$ and $\vec{S_g}$ are the target and the background velocity vector. The circling wind velocity and migrating wind velocity are first summed up to obtain the simulated wind velocity. The coefficient r is obtained by the distance and the radius of the maximum wind speed. After data assimilation, the credited wind field is obtained.

FVCOM is utilized to simulate the tidal evolution. FVCOM is an unstructured-grid, finite-volume model that represents the dynamic process based on the governed equations (Chen et al., 2006). FVCOM has continually been developed and enhanced with a diversity of functions (Zhang et al., 2020). The wet/dry treatments component, the unstructured grid component, and the parallel computation component are essential functions that facilitate the FVCOM model to simulate the storm surge hazard.

For the simulation requirement, the computational region is from $105.73°$E to $125.04°$E in longitude and from $15.41°$N to $28.35°$N in latitude. As shown in Figure 4-(c), the research area is from Zhejiang Province, China, to Vietnam and the Philippines which covers most parts of the South Sea. An unstructured grid including $180,228$ nodes and $355,047$ triangle elements is designed to cover the whole research region as in Figure 4-(a). The spatial resolution of the Shenzhen area and other cities in Guangdong Province is about 500 meters and $1,000$ meters, respectively. The spatial resolution for the remaining area is about 30 km (shown in Figure 4-(b)). The southeast board is the open boundary for the tidal simulation. The water levels of the open boundary are obtained according to the TPXO9-atlas data.

As shown in Figure 5, the elevation of the complex topography in the research region is from $-6,600.55$ meters to $1,096.93$ meters when the elevation of the sea level is 0 meters. The deepest region is in the southeast area, close to the Philippines. The adjacent nodes face the situation that the elevations can differ greatly due to the large spatial resolution of the grid. These issues can be an obstacle to other convergence of the FVCOM model. Thus, elevation interpolation is necessary. The interpolation method is shown as follows.

$$d_i = \gamma * (\textstyle\sum_j d_j)/N + (1-\gamma) * d_i \\ d_i, d_j \in Tr, i \neq j \tag{6}$$

where Tr represents the triangle elements in the grids. d_i and d_j represent the elevation of the target node and its adjacent nodes. N represents the number of adjacent nodes for the target node d_i. γ represents the interpolation rate to smooth the topography. The topography is smooth by the elevation of the neighbors.

After tackling the issues in the tidal and wind field simulation, the Jelesnianski model and the FVCOM model have to be coupled together for storm surge hazard simulation. The Jelesnianski model generates the wind field based on the resolution of the background wind field, CCMP, then after the data fusion, the wind field from time to time is obtained and can be fed into the FVCOM. The grid utilized in the FVCOM is the unstructured grid, which is different from the grid of the wind field. The wind field data have to be interpolated for simulation convenience. Then, the coupled numerical simulation method can reproduce the inundation process of the hazard.

4.3 A differential semi-quantitative storm surge assessment method

As extreme meteorological and hydrological activities cause enormous amounts of seawater to crash onto the land, urban in-

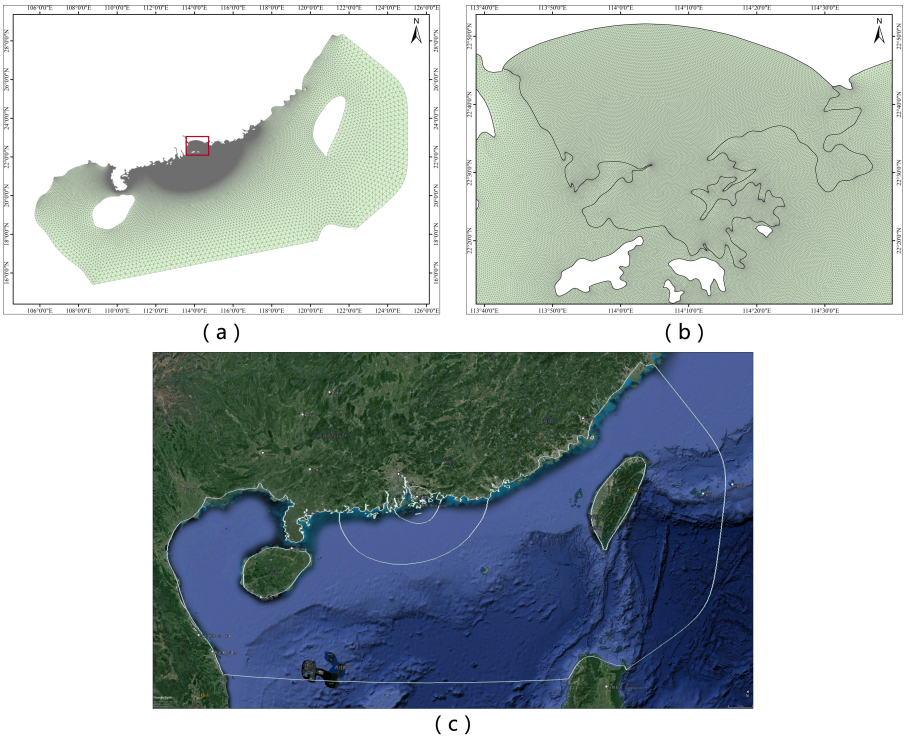

Figure 4. The grid of the overall simulation domain (a) and the study area, Shenzhen (b). The satellite image and the boarder in this research (c) was obtained from Google Earth ©Google Earth.

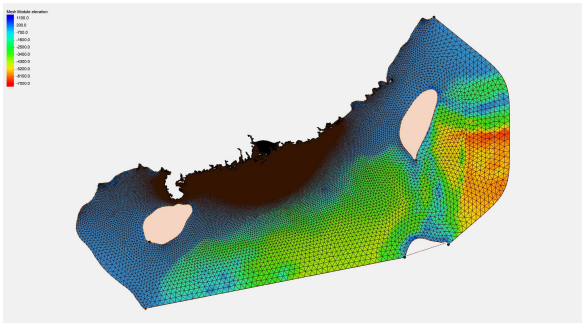

Figure 5. The topography and the bathymetry of the south sea.

undation requires assessment. The sufficient simulation calculates the water depth in the high spatial and temporal resolution that gives the possibility to the elaborate hazard assessment.

Vulnerability of urban infrastructure, the intensity of storm surge inundation, and the risk of the corresponding disaster are three vital indices required for assessment (Beven et al., 2018). The vulnerability index is utilized to classify the LULCs in the coastal region based on their different types and functions. The disaster intensity index is to evaluate the harmless of urban inundation in a storm surge which is determined by the water depth. The risk index assesses the stricken situation for each LULC, as concluded by the vulnerability and disaster intensity indices.

"Guideline for Risk Assessment and Zoning of Storm Surge Disaster" was proposed by the State Oceanic Administration in 2016. In the guideline report, the storm surge hazard assessment standard is stipulated in detail. Based on these principles, the assessment methodology is extended for the storm surge hazard in this paper.

For the vulnerability differentiated assessment, the corresponding relationships between the LULC types and the vulnerability index are presented in Table 1. The LULC data are classified into 5 types, including residential, commercial, industrial, transportation, and public management and service (Gong et al., 2020). One or more sub-categories are classified for the elaborate LULC analysis. However, based on the traditional method, the vulnerability is entirely the same for the same type of LULCs. For example, the degrees of popularity or the recency can vary the same type LULCs. In this paper, combined with POI data, vulnerability can be redefined by the proposed differential semi-quantitative assessment method.

$$\begin{aligned} \kappa_c &= N_c / \max(N_c), N_c = \{N_{c1}, N_{c2}, \ldots, N_{cb}\} \\ \hat{U}_c &= \{U_c - \kappa_{c1} + 0.5, U_c - \kappa_{c2} + 0.5, \ldots, U_c - \kappa_{cb} + 0.5\} \end{aligned} \tag{7}$$

where N_c represents the number of POIs in each LULC area. κ_c represents the importance index of each LULC. The number of POIs located in a LULC stands for the importance of the LULC among the same type of LULC. The range of κ_c is from 0 to 1, and the higher the number, the greater the importance. U_c represents the official vulnerability index for LULC c. Based on Eqation 7, not only the POI data is mapped to the LULC data, but the vulnerability assessment method is extended from 4 levels to an indiscrete value from 0.5 to 4.5. The vulnerabilities of the same LULCs are correspondingly evaluated by leveraging the new importance index κ_c.

The danger of the hazard is assessed based on the principle shown in the Table 2. There are four levels that are defined by the inundation depth. Level I represents that the inundated depth is over 300 cm, and level IV represents that the inundation depth is above 15 cm and less than 50 cm. The inundation depth of each LULC is determined by the nearest neighbor theory according to the distance between the grid node and the LULC location.

Table 1. The land use and land cover type and its corresponding vulnerability value and level.

Level 1		Level 2			Vulnerability	
No	Class name	No	Class name	Description	Index	Level
1	Residential	1-a	Residential	Residential housing, used for live.	1	I
2	Commercial	2-a	Business office	Commercial office buildings for finance, Internet technique, media, etc.	0.8	II
		2-b	Commercial Service	Malls for commercial retails, restaurants, entertainments, etc.	0.9∼1	I
3	Industrial	3-a	Industrial	Factories for industrial production, including mining, manufacturing, etc.	0.6∼1	I∼II
4	Transportation	4-a	Road	Freeways, major and minor-roads.	0.6∼0.8	II
		4-b	Transportation stations	Infrastructure for the transportation, including subway, motor, bus, train, etc.	0.8∼1	I∼II
		4-c	Airport facilities	Airports for plane land and departure.	0.8∼1	I∼II
5	Public management & service	5-a	Administrative	Government and public services area.	1	I
		5-b	Educational	Schools, Universities, institutes.	1	I
		5-c	Medical	Hospital and emergency services	1	I
		5-d	Sport & cultural	Gym center, libraries, museums, exhibition center, etc.	0.6	II
		5-e	Park & greenspace	Park and greenspace covered by plants and trees.	0.4	III

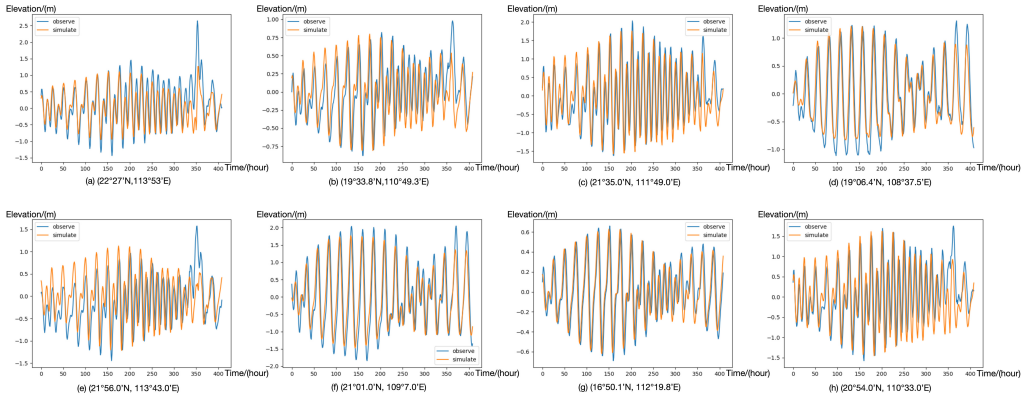

Figure 6. Compared to 8 tide station, the simulation results and the measurement data are presented in these figures.

Table 2. The officially risk assessment standard.

Danger level	Inundated depth (cm)
I	[300, $+\infty$)
II	[120, 300)
III	[50, 120)
IV	[15, 50)

Based on the danger and vulnerability of the hazard, the risk can be calculated by the multiplication of U_c and G_c. G represents the danger of the LULC area c. The range of the vulnerability is from 0.5 to 4.5. The range of the danger includes levels I, II, III, and IV. Thus the range of the risk index is from 0.5 to 18. Note that a lower risk index value represents higher hazard risks for the LULC.

By the proposed assessment method, the vulnerability of the urban LULC, the danger, and the risk of the hazard are correspondingly assessed. The indiscrete index in the assessment can elaborate the hazard evaluation. In conclusion, from simulation to assessment, the proposed digital twin system achieves the hazard digitalization, and the simulation results support hazard prevention.

5. CASE STUDY

To verify the effectiveness of the proposed DSURAM, a case study was conducted to reproduce a storm surge Mangkhut in Shenzhen. Details of the case are presented in Section 5.1 and 5.2.

5.1 Experimental setup

Storm surge Mangkhut hit Guangdong Province on 16 September 2018. It was generated at the northwest of the Pacific Ocean on 7 September 2018. Its trajectory passed through Japan, north Philippines, and eventually dissipated at Guangxi Province, China. When landing at Guangdong Province, the wind speed approached level 14 based on the Beaufort scale, and the minimum center air pressure was 955 hPa.

The simulation for storm surge Mangkhut ran from 1 September 2018 to 19 September 2018. The simulation time interval was customized to 3 seconds. The data processing was implemented in Matlab and Python. Simulation was executed on a workbench with 3.6-GHZ octa-core, and 8-GB DRAM memory. Assessment was executed on a workbench with 3.6-GHZ sixteen-core and 32-GB DRAM memory.

To verify the effectiveness of the simulation method, the output of the numerical method was compared to the elevation data collected by the tide station. The accuracy of the simulation result was calculated by the Mean Square Error (MSE) method.

5.2 Experimental results

Based on the storm surge Mangkhut related data, the Jelesnianski model, and background data, CCMP, reproduced the wind

field information as shown in Figure 7. The status of the wind field and the air pressure is illustrated in this figure. It can be seemed that the circling wind velocity plays the dominant role when the location is close to the storm surge center. From 12 : 00 to 15 : 00 on 17 September 2018, the storm surge intensity gradually decreased.

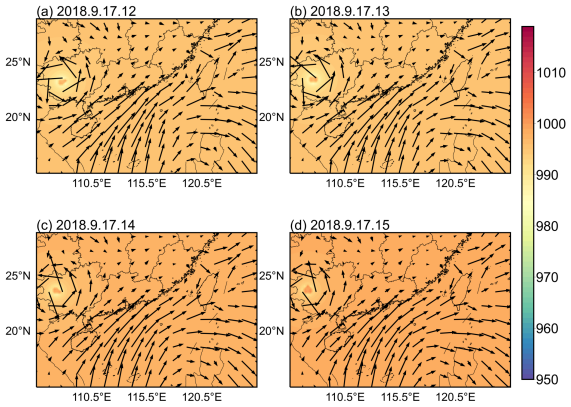

Figure 7. The wind field for storm surge Mangkhut after assimilation. (a)-(d) present the wind field from 12 : 00 to 15 : 00 in 17 September 2018.

After the wind field was well prepared, the FVCOM model was utilized to simulate the marine evolution during storm surge Mangkhut. The simulation result is shown as Figure 6. Data from 8 tide stations are utilized to verify the simulation results. The verification started from 1 September 2018, 12 : 00 to 19 September 2018, 0 : 00. The absolution error, the relative error, and the MSE of the simulation are 0.353 meters, 0.183, and 0.289 meters, respectively. The inundation in Shenzhen is shown as Figure 8. The southwest coast, which is the economic and population center of Shenzhen, was severely affected. The flooding area in the southeast is a new district, and residents are converged in the center of this area. Thus, hazard losses were mostly at the west and the southwest area of Shenzhen.

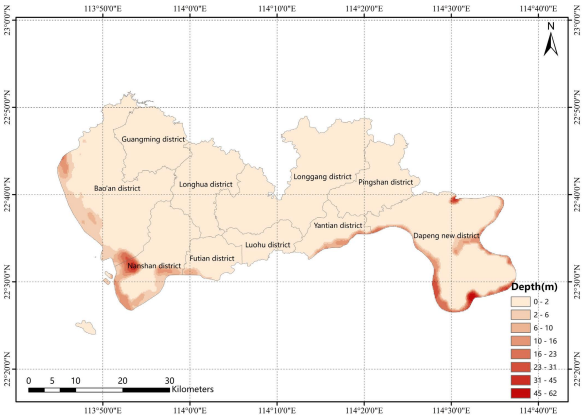

Figure 8. The simulated inrush sea water distribution status caused by storm surge Mangkhut.

A multi-scale risk assessment was conducted based on the inundation status in the urban area. Figure 9, Figure 10, and Figure 11 present the vulnerability, danger, and risk assessment results, respectively. As shown in Figure 9, building distributions in the southwest and west coasts are extremely crowded, and the vulnerability of most LULCs is less than 2.0. As shown in Figure 10, along the west coastline, LULCs are under the threat of seawater. For danger levels I to IV, there are 146, 251, 126, and 111 LULCs, respectively. Among the 5 districts, Bao'an district is in the most danger, including 434 LULCs in danger. 208 LULCs in Bao'an district are suffering level II danger from the hazard. Figure 8 shows that, massive seawater flows into the Dapeng new district, but a low number of LULCs prevents the same loss as Nanshan district and Bao'an district. Note that LULCs in danger in Yantian district are mostly at level I ($84.78\% = \frac{39}{39+7}$).

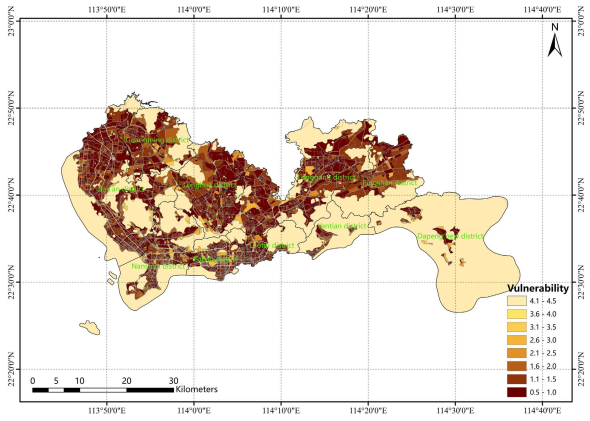

Figure 9. The vulnerability of LULCs in the Shenzhen area for storm surge hazard.

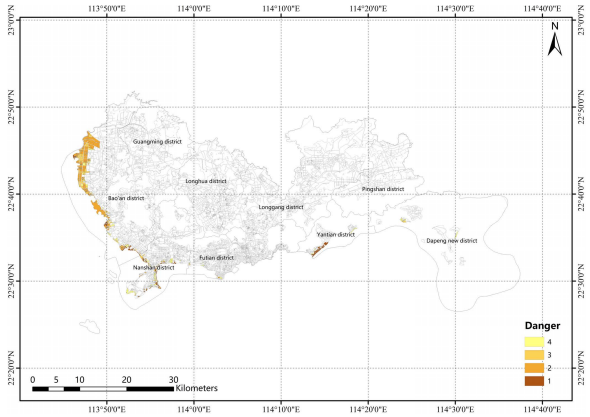

Figure 10. The danger assessment of LULCs in the Shenzhen area for storm surge hazard Mangkhut.

Comprehensively analyzing the vulnerability and the danger above, the risk assessment is obtained in Figure 11. Due to the vulnerability, even though some LULCs in the west area are in level 1 to level 3 while assessing the danger index, these LULCs become the highest risk areas in risk assessment. If $4.5 = 18/4$ is selected as threshold to present the hard-hit areas in the storm surge Mangkhut, there are respectively 344 and 87 LULCs in the Bao'an district and the Nanshan district whose risk index less than 4.5. The airport facilities, educational and medical services are influenced in these two districts. There are 149, 106, and 76 resident buildings, commercial services and industries that are severely stricken. These three LULC types occupies more than half of the total affected LULCs. Note that there are 27 medical services and 22 educational services are in serious risks in the storm surge Mangkhut.

6. CONCLUSION

In light of storm surge inundation regulatory analysis and prevention requirements, a DSURAM is proposed to simulate the

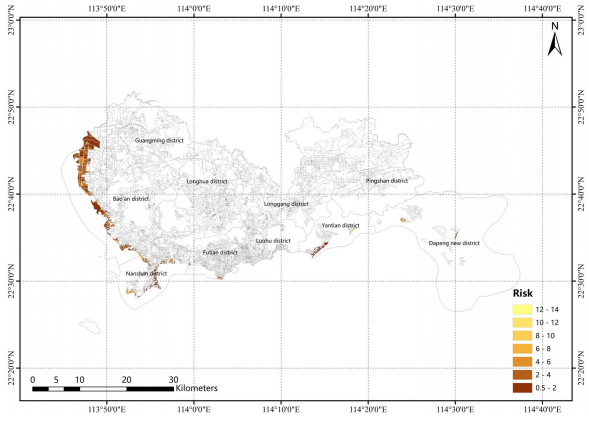

Figure 11. The risk assessment of LULC in Shenzhen area for storm surge hazard Mangkhut

inundation evolution and assess the risk to coastal cities. Under the concept of the digital twin, the storm surge model was designed to embed the simulation and the assessment in a complete technical framework. The storm surge reproduces architecture by coupling the wind field model, the Jelesnianski model, and the numerical model, FVCOM. The proposed differentiated semi-quantitative risk assessment method is driven by multi-source urban data based on an official standard. A case study of storm surge Mangkhut in 2018 was conducted in this work. A storm surge digital twin system was built to simulate the storm surge Mangkhut and assess the vulnerability, danger, and risk of this hazard. The case study proves that the proposed method can effectively analyze high-intensity storm surges.

ACKNOWLEDGMENT

This work is funded by the National Natural Science Foundation of China (U1711266 and No. 41925007), the Strategic Priority Research Program of the Chinese Academy of Sciences, grant number XDA19090128, and Hubei Natural Science Foundation of China (No. 2019CFA023).

REFERENCES

Beven, K. J., Almeida, S., Aspinall, W. P., Bates, P. D., Blazkova, S., Borgomeo, E., Freer, J., Goda, K., Hall, J. W., Phillips, J. C. et al., 2018. Epistemic uncertainties and natural hazard risk assessment–Part 1: A review of different natural hazard areas. *Natural Hazards and Earth System Sciences*, 18(10), 2741–2768.

Ceres, R. L., Forest, C. E., Keller, K., 2017. Understanding the detectability of potential changes to the 100-year peak storm surge. *Climatic Change*, 145(1), 221–235.

Chen, C., Beardsley, R., Cowles, G., 2006. An unstructured grid, finite-volume coastal ocean model (FVCOM) system. Special issue entitled "advance in computational oceanography". *Oceanography*, 19(1), 78-89.

Chen, S., BAI, N., 2011. Effect Analysis of Water Depth Measurement Error on Discharge Date Reorganization Accuracy [D]. *Heilongjiang Science and Technology of Water Conservancy*, 4.

Dube, S., Chittibabu, P., Sinha, P., Rao, A., Murty, T., 2004. Numerical modelling of storm surge in the head Bay of Bengal using location specific model. *Natural Hazards*, 31(2), 437–453.

E, G. H., E, N. D., 1959. Meteorological considerations pertinent to standard project hurricane,Atlantic and Gulf coasts of the United States. *National Hurriane Research Project Report*, 33(1), 20-39.

Egbert, G. D., Erofeeva, S. Y., 2002. Efficient inverse modeling of barotropic ocean tides. *Journal of Atmospheric and Oceanic technology*, 19(2), 183–204.

Fuller, A., Fan, Z., Day, C., Barlow, C., 2020. Digital twin: Enabling technologies, challenges and open research. *IEEE access*, 8, 108952–108971.

Gong, P., Chen, B., Li, X., Liu, H., Wang, J., Bai, Y., Chen, J., Chen, X., Fang, L., Feng, S. et al., 2020. Mapping essential urban land use categories in China (EULUC-China): preliminary results for 2018. *Science Bulletin*, 65(3), 182–187.

Hinkel, J., Lincke, D., Vafeidis, A. T., Perrette, M., Nicholls, R. J., Tol, R. S., Marzeion, B., Fettweis, X., Ionescu, C., Levermann, A., 2014. Coastal flood damage and adaptation costs under 21st century sea-level rise. *Proceedings of the National Academy of Sciences*, 111(9), 3292–3297.

Kapoor, D., 1981. General bathymetric chart of the oceans (GEBCO). *Marine Geodesy*, 5(1), 73–80.

Liu, Y., Lu, C., Yang, X., Wang, Z., Liu, B., 2020. Fine-Scale Coastal Storm Surge Disaster Vulnerability and Risk Assessment Model: A Case Study of Laizhou Bay, China. *Remote Sensing*, 12(8), 1301.

McGranahan, G., Balk, D., Anderson, B., 2007. The rising tide: assessing the risks of climate change and human settlements in low elevation coastal zones. *Environment and urbanization*, 19(1), 17–37.

Polomčić, D., Bajić, D., Ratković, J., 2018. Assessment of Historical Flood Risk to the Groundwater Regime: Case Study of the Kolubara Coal Basin, Serbia. *Water*, 10(5), 588.

Shen, H.-Y., Chang, L.-C., 2013. Online multistep-ahead inundation depth forecasts by recurrent NARX networks. *Hydrology and Earth System Sciences*, 17(3), 935–945.

Shi, H., You, Z., Hu, C., Li, Q., Deyun, W., Xie, P., 2018. Study on the Applicability of Different Typhoon Synthetic Wind Field Schemes in the South China Sea. *Transactions of Oceanology and Limnology*, 6(7), 17-23.

Wessel, P., Smith, W. H., 1996. A global, self-consistent, hierarchical, high-resolution shoreline database. *Journal of Geophysical Research: Solid Earth*, 101(B4), 8741–8743.

Xianwu, S., Jufei, Q., Bingrui, C., Xiaojie, Z., Haoshuang, G., Jun, W., Zhuyuan, B., 2020. Storm surge risk assessment method for a coastal county in China: case study of Jinshan District, Shanghai. *Stochastic Environmental Research and Risk Assessment*, 34(5), 627–640.

Zachry, B. C., Booth, W. J., Rhome, J. R., Sharon, T. M., 2015. A National View of Storm Surge Risk and Inundation. *Weather, Climate, and Society*, 7(2), 109–117.

Zhang, J., Chen, Y., 2019. Risk assessment of flood disaster induced by typhoon rainstorms in Guangdong province, China. *Sustainability*, 11(10), 2738.

Zhang, Y., Chen, C., Beardsley, R. C., Perrie, W., Gao, G., Zhang, Y., Qi, J., Lin, H., 2020. Applications of an unstructured grid surface wave model (FVCOM-SWAVE) to the Arctic Ocean: The interaction between ocean waves and sea ice. *Ocean Modelling*, 145, 101532.

Zheng, Z., Huang, D., Zhang, J., He, S., Liu, Z., 2010. A soa-based decision support geographic information system for storm disaster assessment. *2010 18th International Conference on Geoinformatics*, IEEE, 1–6.